Geophysical Research Letters

Supporting Information for

The influence of the trend, basin interactions and ocean dynamics on tropical ocean prediction

Michael A. Alexander[1], Sang-Ik Shin[1,2], and David S. Battisti[3]

[1]NOAA Physical Sciences Laboratory, Boulder, CO, USA

[2] CIRES, University of Colorado Boulder, Boulder, CO USA

[3]Department of Atmospheric Sciences, University of Washington, Seattle, Washington.

Contents of this file in order

Text S1: Filter design for the trend and ENSO

S1.1 Empirical Normal Modes

Following Penland and Matrosova (1996) and Compo and Sardeshmukh (2010), we can use the LIM framework to design filters for the trend and ENSO-related variability. Empirical Normal Modes (ENMs, also known as Principal Oscillation Patterns; Penland and Ghil 1993; von Storch et al. 1995; Penland and Matrosova 2006) are the solution of the homogeneous part of LIM, $\mathrm{d}\mathbf{x}/\mathrm{d}t = \mathbf{L}\mathbf{x}$. The ENMs can be expressed as:

$$\mathbf{x}_j(t) = \mathbf{u}_j \exp(\beta_j t) c_j \text{ and } \beta_j = \sigma_j + i\omega_j,$$

where $\mathbf{u}_j$ and β_j are the *j*-th eigenvector and eigenvalue of $\mathbf{L}$, and c_j is an arbitary complex constant. The eigenvalue includes information on the damping timescale ($-1/\sigma_j$) and the period ($2\pi/\omega_j$). ENMs can either be a single damped non-oscillatory mode or a pair of damped modes that oscillate at a set period. By using ENMs, the state vector **x** can be reconstructed as:

$$\mathbf{x}(t) = \sum_j z_j \mathbf{u}_j \text{ , and } z_j = \mathbf{v}_j^{\mathrm{T}} \mathbf{x}(t), \tag{S1}$$

where, $\mathbf{u}_j$ is the *j*-th eigenvector of $\mathbf{L}$ (i.e., *j*-th ENM) and $\mathbf{v}_j$ is the corresponding modal adjoint (i.e., the *j*-th eigenvector of $\mathbf{L}^{\mathrm{T}}$). The $\mathbf{u}_j$ and $\mathbf{v}_j$ share the common eigenvalue β_j that represents the period [$2\pi/\mathrm{Im}(\beta_j)$] and decay time [$-1/\mathrm{Re}(\beta_j)$] of the *j*-th ENM.

The ENM damping timescales and periods are given in Table S1. The first ENM is non-oscillatory and very weakly damped ($-1/\sigma_j$ = 103 months); it represents the long-term trend with strong warming except in the central and eastern equatorial Pacific (Figure S1), i.e.

$$\mathbf{x}(t) = \underbrace{z_1 \mathbf{u}_1}_{\substack{\| \\ \text{Least Damped Mode} \\ \mathbf{x}_{\text{Trend}}(t)}} + \sum_{j \neq 1} z_j \mathbf{u}_j . \tag{S2}$$

Table S1. Damping timescales and Periods of the 30 empirical normal modes (ENMs). ENMs are ranked by their decay timescales.

ENM	Damping Timescale (Month)	Period (Month)	Comments
1	103.1	∞	Trend
2	24.7	∞	
3	21.4	∞	
4/5	11.1	45.4	ENSO
6	10.8	∞	
7/8	9.3	76.9	
9/10	7.8	34.7	ENSO
11	7.6	∞	
12	5.7	∞	
13/14	5.6	47.1	
15/16	5.4	22.5	
17	5.1	∞	
18/19	4.6	105.9	
20/21	4.3	22.3	
22	3.2	∞	
23/24	3.1	51.3	
25	2.5	∞	
26/27	2.2	23.2	
28	1.8	∞	
29/30	1.7	55.9	

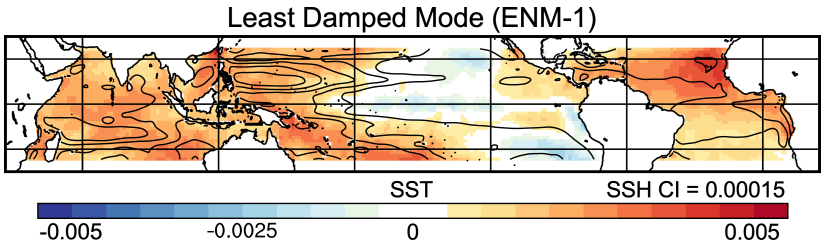

Figure S1: Pattern of least damped mode (ENM-1). Shading: SST, Contour: SSH. The contour intervals are arbitrary.

Text S1.2 Optimal Structure

Though its dynamics are stable, the LIM anomalies can undergo growth over finite time intervals via modal interference. This growth can be diagnosed through the SVD of $\mathbf{G}(\tau)$ under the L2-norm (Euclidean norm) of $\mathbf{L}$ or of any of its submatrices, which yields pairs of singular vectors (SVs) $\mathbf{u}_\kappa$ and $\mathbf{v}_\kappa$ [κ=1, 2, …, 30 (rank of $\mathbf{G}$)] with unit amplitude and singular values λ_κ (e.g., Farrell 1988; Lacarra and Talagrand 1988; PS95; Vimont et al. 2014). Ordering the SVs by decreasing singular value, if $\mathbf{x}(t) = \alpha \mathbf{v}_1$, then $\mathbf{x}(t+\tau) = \mathbf{G}(\tau) \cdot \alpha \mathbf{v}_1 = \alpha \lambda_1 \mathbf{u}_1$. That is, over the time interval [t, $t+\tau$], the maximum increase in domain-integrated variance occurs when $\mathbf{x}(t)$ is proportional to the leading right singular vector $\mathbf{v}_1$, or the "optimal initial perturbation," with the "maximum amplification" factor $\lambda_1^2(\tau)$. Here the optimal structure is based on the SST Euclidian (L2) norm in the Pacific. The maximum amplification (MA) curves under the L2 norm of tropical Pacific SST submatrix, optimal initial structure, and evolved structure at 6, 12, 18, and 24 months are shown in Figure S2. The optimal structure of SST is similar to that in the SST-only LIM (e.g., Penland and Sardeshmukh 1995). Here we include SSH as well as SST in the LIM, since SSH provides a key measure of ocean dynamics and has been shown to enhance the skill of SST forecasts over SST-only LIMs (Newman and Sardeshmukh 2017; Shin et al. 2021). The optimal structure and its SST and SSH evolution are consistent with the patterns associated with the Delayed Oscillator and Recharge Oscillator hypotheses for ENSO (e.g., Battisti and Hirst, 1989; Jin 1997; Meinen and McPhaden, 2000).

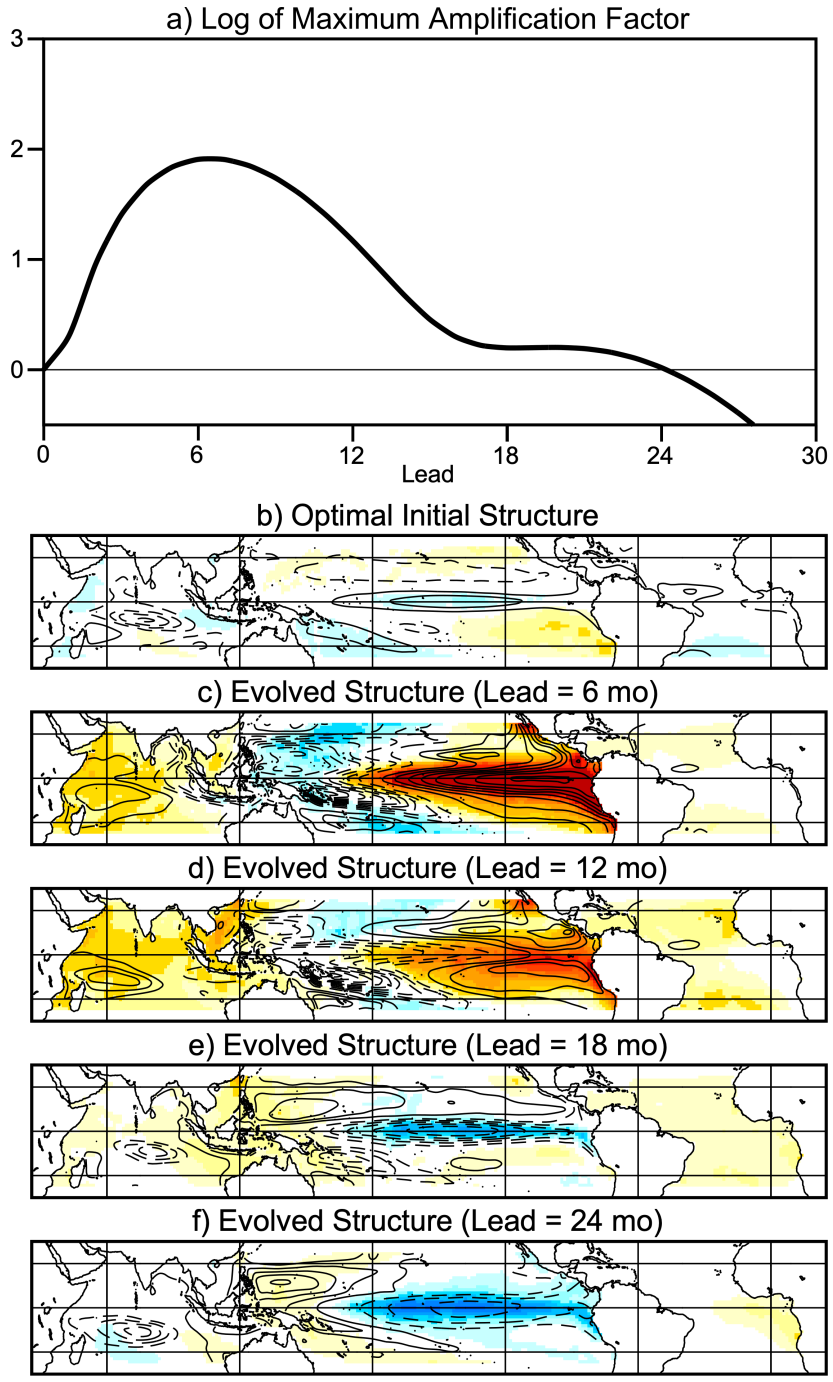

Figure S2: (a) Maximum amplification curve. (b) Optimal initial structure and its evolved structure at (c) 6, (d)12, (e)18, and (f)24 months

Text S1.3 Non-normal ENSO filter

To remove the propagating ENSO signal, we will further decompose (S2) as a trend, ENSO-related, and residuals, i.e.

$$\mathbf{x}(t) = \underbrace{z_1\mathbf{u}_1}_{\substack{\| \\ \text{Least Damped Mode} \\ \mathbf{x}_{\text{Trend}}(t)}} + \sum_{j\in\text{ENSO}} z_j\mathbf{u}_j + \sum_{j\notin\{\text{ENSO},1\}} z_j\mathbf{u}_j \,. \tag{S3}$$

For the criteria of ENSO-related mode selection, we followed the procedure described by Penland and Matrosova (2006). The procedure is 1) estimate the contribution of each ENM to the propagating ENSO-like signal by projecting the modal adjoint $\mathbf{v}_j$ onto the optimal structure (Fig. S1b), and 2) select the dominant ENM pairs and assign these modes as ENSO-related. Note that lag covariance based $\mathbf{L}$ is asymmetric, so that the model adjoints are often complex conjugate pairs.

Figure S3a shows the projection coefficients, where two oscillating ENM pairs (ENMs 4/5 and 9/10) are particularly relevant in explaining LIM's optimal ENSO growth. The ENSO-related ENM patterns are shown in Fig S3b, and, in Fig. S4, we compare the ENSO-filtered Niño 3.4 time series with the unfiltered and untruncated (in EOF space) time series, as well as their power spectra. The filtering greatly reduces the SST anomalies in the strong El Niño years of 1972-73, 1982-83, 1986-87, and 1997-98 and reduces the variance in the spectra on the ENSO timescale of approximately 2-7 years. We note that filtering enhanced the negative SST anomalies during the 1999 La Niña, indicating that the filter may not have removed the ENSO signal during this period. However, the cooling may be partly attributable to a random event or cyclic phenomena not associated with ENSO.

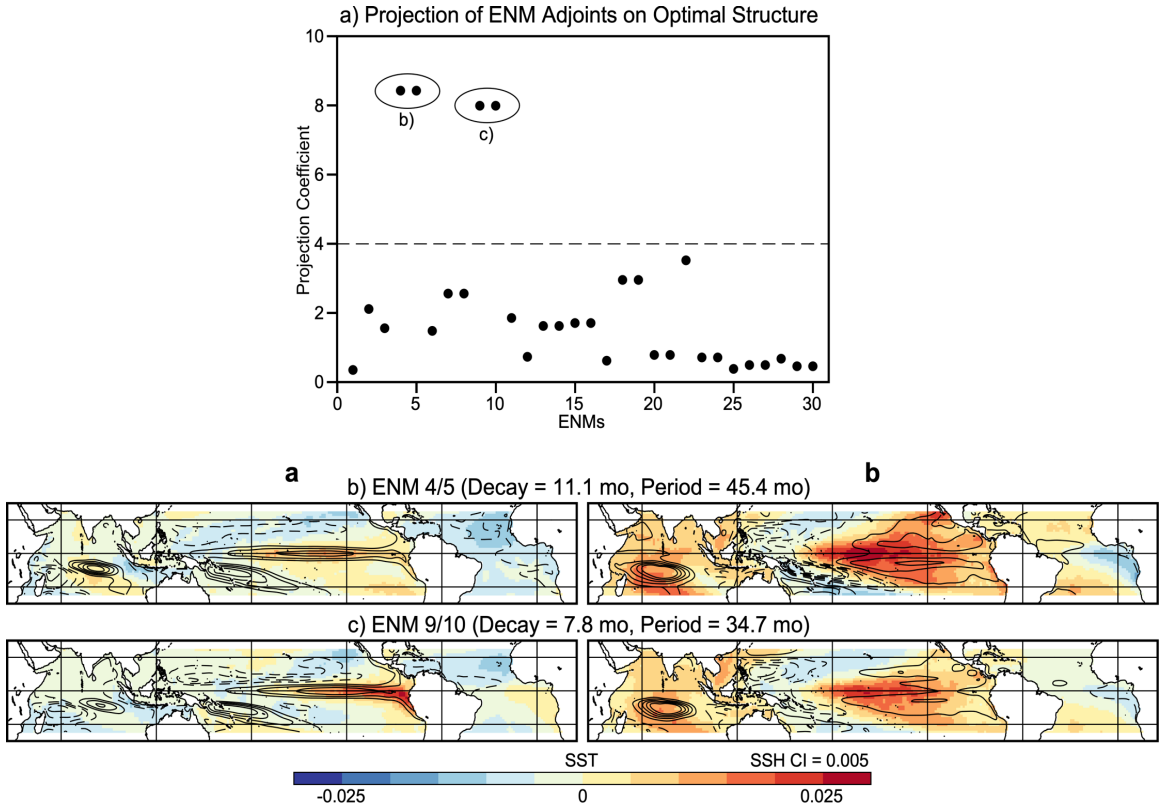

Figure S3. a) Magnitude of projection of optimal initial structure onto the empirical normal mode adjoints. Modes 4/5 and 8/9 project strongly onto the adjoints of the optimal structure. b) and c) Patterns of the ENSO-related ENMs. The pairs of modes evolve from **a** → **b** → **-a** → **-b** → **a** over its period. ENMs 4/5 (9/10) have a period of 45.4 (34.7) months and a decay time of 11.1 (7.8) months. The SST has a shading interval of 0.005, and the SSH has a contour interval of 0.005.

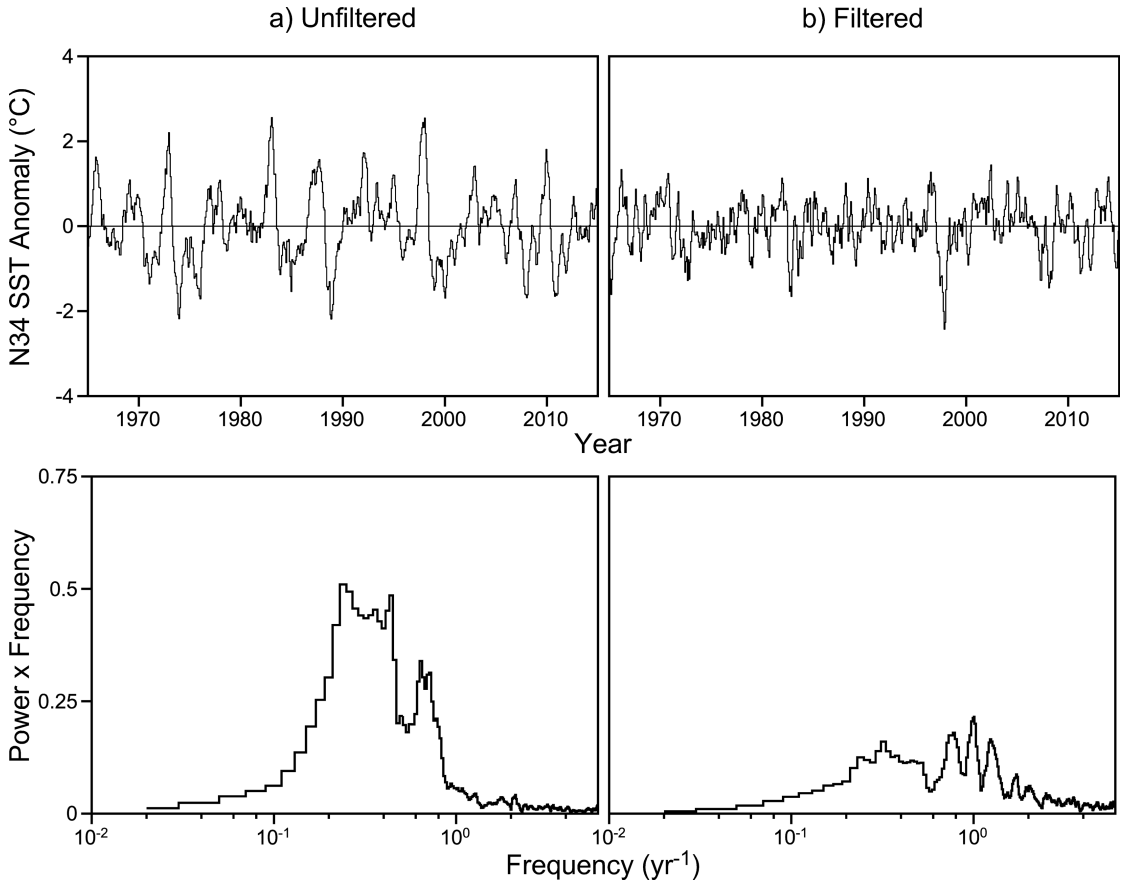

Figure S4. a) Nino3.4 SST anomaly time series (top) and power spectra (bottom). b) The same as a) but for the ENSO-filtered SST anomalies. The SST anomalies were filtered by removing the SST anomalies with ENMS 4/5 and 9/10.

Table S2. Damping timescales of ENM-1 during the cross-validation procedure and the pattern correlations between ten cross-validated cases and the entire 50-yr case.

		10% (5 yr) Withholding Period									
		1965 - 1969	1970 - 1974	1975 - 1979	1980 - 1984	1985 - 1989	1990 - 1994	1995 - 1999	2000 - 2004	2005 - 2009	2010 - 2014
Damping Time Scale (mo)		105.7	125.1	106.0	114.3	122.9	133.7	131.4	119.2	63.1	61.1
Pattern Correlation with ENM-1 in Figure S1	SST	0.98	0.98	0.98	0.99	0.99	0.98	0.99	0.99	0.96	0.92
	SSH	0.99	0.99	0.99	1.0	1.0	0.99	1.0	1.0	0.97	0.92

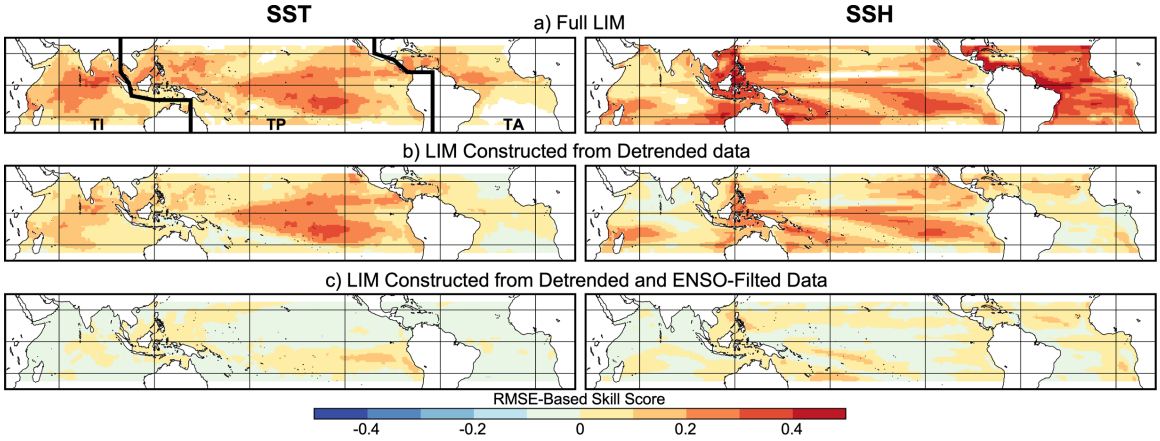

Figure S5. Hindcast skill as indicated by the RMSE-based skill score (RMSSS) between the six-month lead LIM forecasts and observations for SST (left) and SSH (right) over 1964-2004. (a) full LIM, (b) LIM constructed from detrended data (removal of ENM 1), and (c) LIM constructed from detrended and ENSO-filtered data (removal of ENM 1, 4/5, and 9/10). (Top left) the tropical Indian (TI), Pacific (TP), and Atlantic (TA) ocean domains are separated by the black lines. Latitude lines are shown at 20°N, 0°, 20°S.

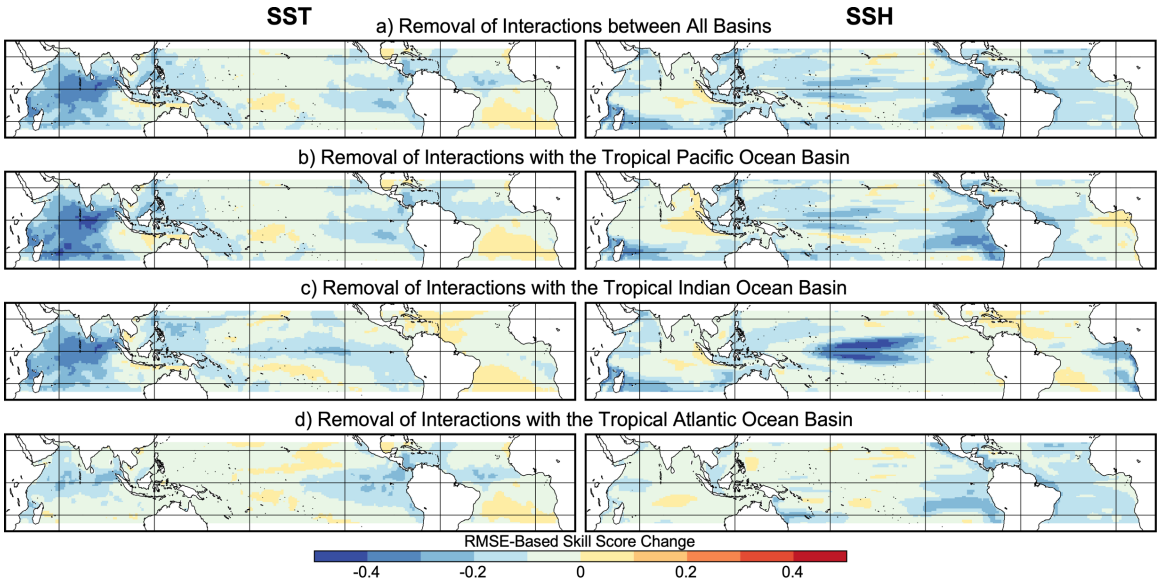

Figure S6. The change in the six-month (left) SST and (right) SSH forecast skill due to basin interactions as indicated by the difference in the RMSSS between the full LIM and LIMs by the removal of all interactions: (a) between all basins; (b) with the tropical Pacific (TP); (c) with tropical Indian (TI). (d) with tropical Atlantic (TA) ocean basins.

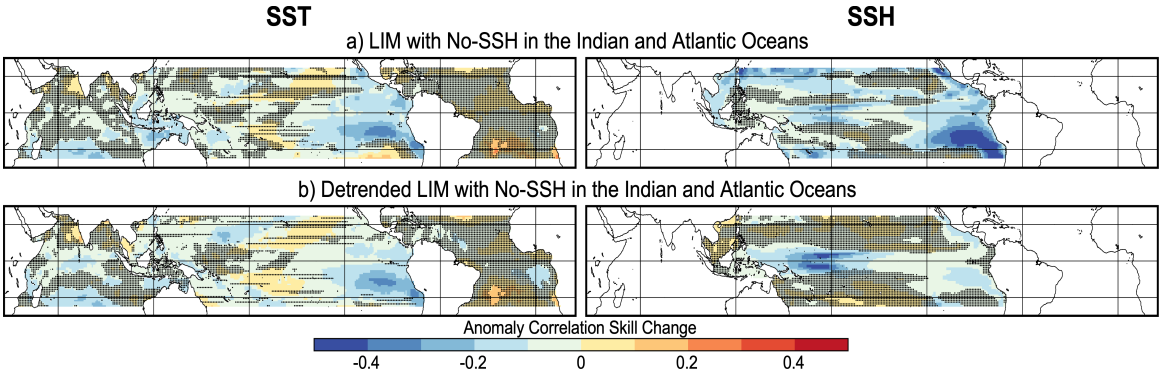

Figure S7. The change in the six-month (left) SST and (right) SSH hindcast skill as indicated by the difference in the RMSSS between the full LIM and a LIM (a) with removal of all SSH terms in the Indian and Atlantic Oceans; (b) using the detrended LIM with no SSH anomalies in the Indian and Atlantic oceans.

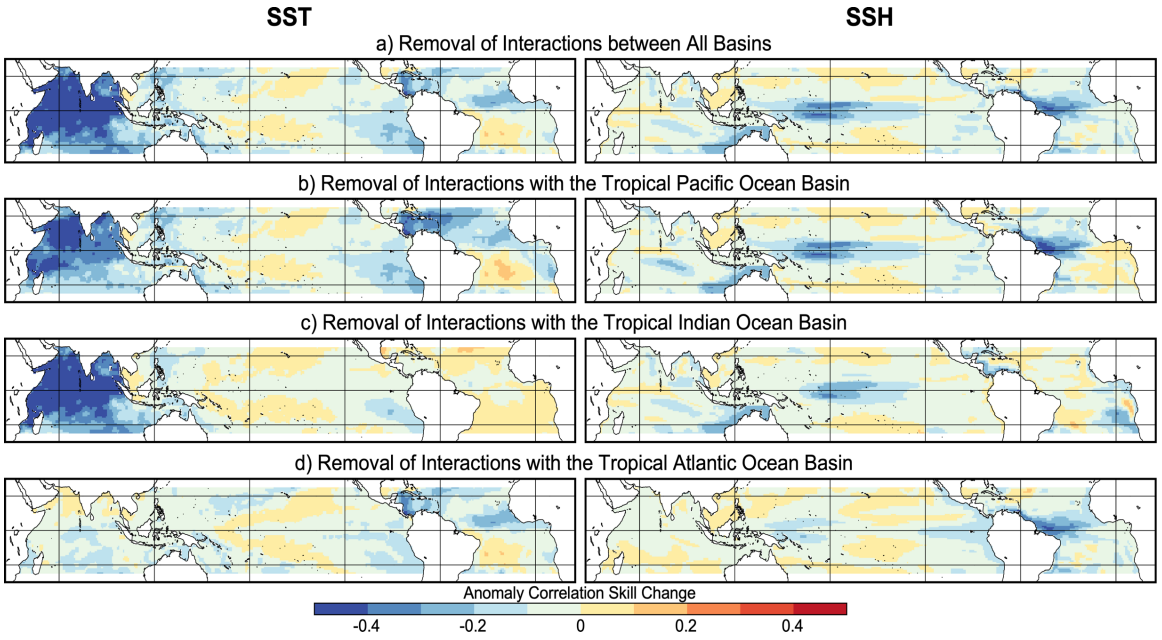

Figure S8. The six-month AC forecast skill as in Figure 2 but with the SST and SSH fields detrended by removing ENM1 and then deriving a new LIM prior to decoupling the basins. Detrending the data first removes some of the coupled interactions as well as the local trend. For example, the long-term warming in the Indian Ocean can impact conditions in the Pacific and Atlantic Oceans.